

Nonmuscle Myosin II Isoforms Coassemble in Living Cells

Jordan R. Beach,^{1,*} Lin Shao,² Kirsten Remmert,¹ Dong Li,² Eric Betzig,² and John A. Hammer III^{1,*}

¹Cell Biology and Physiology Center, National Heart, Lung, and Blood Institute, National Institutes of Health, Bethesda, MD 20892, USA

²Janelia Farm Research Campus, Howard Hughes Medical Institute, Ashburn, VA 20147, USA

Summary

Nonmuscle myosin II (NM II) powers myriad developmental and cellular processes, including embryogenesis, cell migration, and cytokinesis [1]. To exert its functions, monomers of NM II assemble into bipolar filaments that produce a contractile force on the actin cytoskeleton. Mammalian cells express up to three isoforms of NM II (NM IIA, IIB, and IIC), each of which possesses distinct biophysical properties and supports unique as well as redundant cellular functions [2–8]. Despite previous efforts [9–13], it remains unclear whether NM II isoforms assemble in living cells to produce mixed (heterotypic) bipolar filaments or whether filaments consist entirely of a single isoform (homotypic). We addressed this question using fluorescently tagged versions of NM IIA, IIB, and IIC, isoform-specific immunostaining of the endogenous proteins, and two-color total internal reflection fluorescence structured-illumination microscopy, or TIRF-SIM, to visualize individual myosin II bipolar filaments inside cells. We show that NM II isoforms coassemble into heterotypic filaments in a variety of settings, including various types of stress fibers, individual filaments throughout the cell, and the contractile ring. We also show that the differential distribution of NM IIA and NM IIB typically seen in confocal micrographs of well-polarized cells is reflected in the composition of individual bipolar filaments. Interestingly, this differential distribution is less pronounced in freshly spread cells, arguing for the existence of a sorting mechanism acting over time. Together, our work argues that individual NM II isoforms are potentially performing both isoform-specific and isoform-redundant functions while coassembled with other NM II isoforms.

Results and Discussion

TIRF-SIM Reveals Individual NM II Bipolar Filaments

In an initial effort to identify individual nonmuscle myosin II (NM II) bipolar filaments, we expressed NM IIA with an N-terminal EGFP tag (EGFP-NM IIA; note that all tags were fused to the NM II heavy chain; Figure 1A) in U2OS cells and imaged the cells by total internal reflection fluorescence structured-illumination microscopy (TIRF-SIM) (Figure 1C), a TIRF version of a previously established SIM technique [14] that provides two-color imaging capability and achieves a lateral resolution of ~100 nm. This resolution should allow unequivocal identification of ~300 nm NM II bipolar filaments [15, 16], unlike imaging performed by conventional microscopy, where the lateral

resolution is ~250 nm (although see [17]). In TIRF-accessible regions of the lamellar extensions and the cell interior, images revealed what appeared to be individual NM IIA filaments possessing two puncta spaced ~300 nm apart (Figure 1C and insets C1 and C2). These putative filaments were usually embedded in actin networks (Figure 1D and insets D1 and D2) or aligned with linear actin filaments/bundles (Figure 1E and insets E1 and E2) labeled with F-tractin, an F-actin reporter [18, 19]. In regions rich in transverse arcs and ventral stress fibers, however, EGFP-NM IIA puncta were too numerous and close together to identify individual filaments unequivocally (Figure 1C and inset C3). To confirm that these 300 nm-spaced puncta correspond to individual NM IIA bipolar filaments and to resolve these structures in filament-rich regions of the cell, we used NM IIA with a C-terminal mApple tag (NM IIA-mApple; Figure 1A). Because NM II filaments are bipolar, coexpression of NM IIA-mApple with EGFP-NM IIA should result in filaments with EGFP puncta at both ends of the filament (corresponding to the N termini of the head domains) bifurcated by a single mApple punctum (corresponding to C termini of the tail domains) (Figure 1B). Consistently, when these two constructs were coexpressed in U2OS cells, we observed two green puncta ~300 nm apart that were bifurcated by a single red punctum (Figure 1F and inset F1). Moreover, these two-color structures were readily resolvable in filament-rich regions of the cell (Figure 1F and insets F2 and F3). Importantly, the localization of C-terminally tagged NM IIA was qualitatively indistinguishable from N-terminally tagged NM IIA, arguing that the C-terminal tag has no obvious deleterious effects on bipolar filament structure (although minor effects cannot be entirely ruled out). We note that a similar approach employing an N-terminal antibody and a C-terminal fluorophore was used recently to identify bipolar filaments containing NM IIC in epithelia [17].

Exogenous NM II Isoforms Form Heterotypic Filaments

To determine whether NM II isoforms form heterotypic filaments, we coexpressed NM IIA-mApple and EGFP-NM IIB in U2OS cells. Although both isoforms are overexpressed, the ratio of NM IIA to NM IIB in transfected cells remains essentially the same as in untransfected cells (~25:1) because the fold increase over endogenous protein levels is approximately the same for both isoforms (~2.5- to 3-fold) (see Figure S1 and Table S1 available online). Confocal microscopy demonstrated that these two isoforms “colocalize” to some degree throughout most of the cell (Figure 2A), although NM IIA is enriched in peripheral lamella relative to NM IIB, whereas NM IIB is enriched in central and posterior regions relative to NM IIA, as reported by others [8, 20, 21] (see also below). To determine whether this “colocalization” corresponds at least in part to heterotypic filaments of NM IIA and NM IIB, we imaged using TIRF-SIM. Figure 2B shows that the green-red signal expected for heterotypic filaments is indeed very common in TIRF-accessible interior regions of cells (see also insets B1 and B2), although not all puncta conform to this pattern (presumably due to the presence of homotypic filaments, unipolar filaments [22], filaments that are partially out of the TIRF zone, bipolar filaments with a unipolar distribution of one isoform, and/or heterotypic filaments where the signal for one isoform is below the level of detection; see Experimental Procedures for further discussion). Heterotypic

*Correspondence: jordan.beach@nih.gov (J.R.B.), hammerj@nhlbi.nih.gov (J.A.H.)

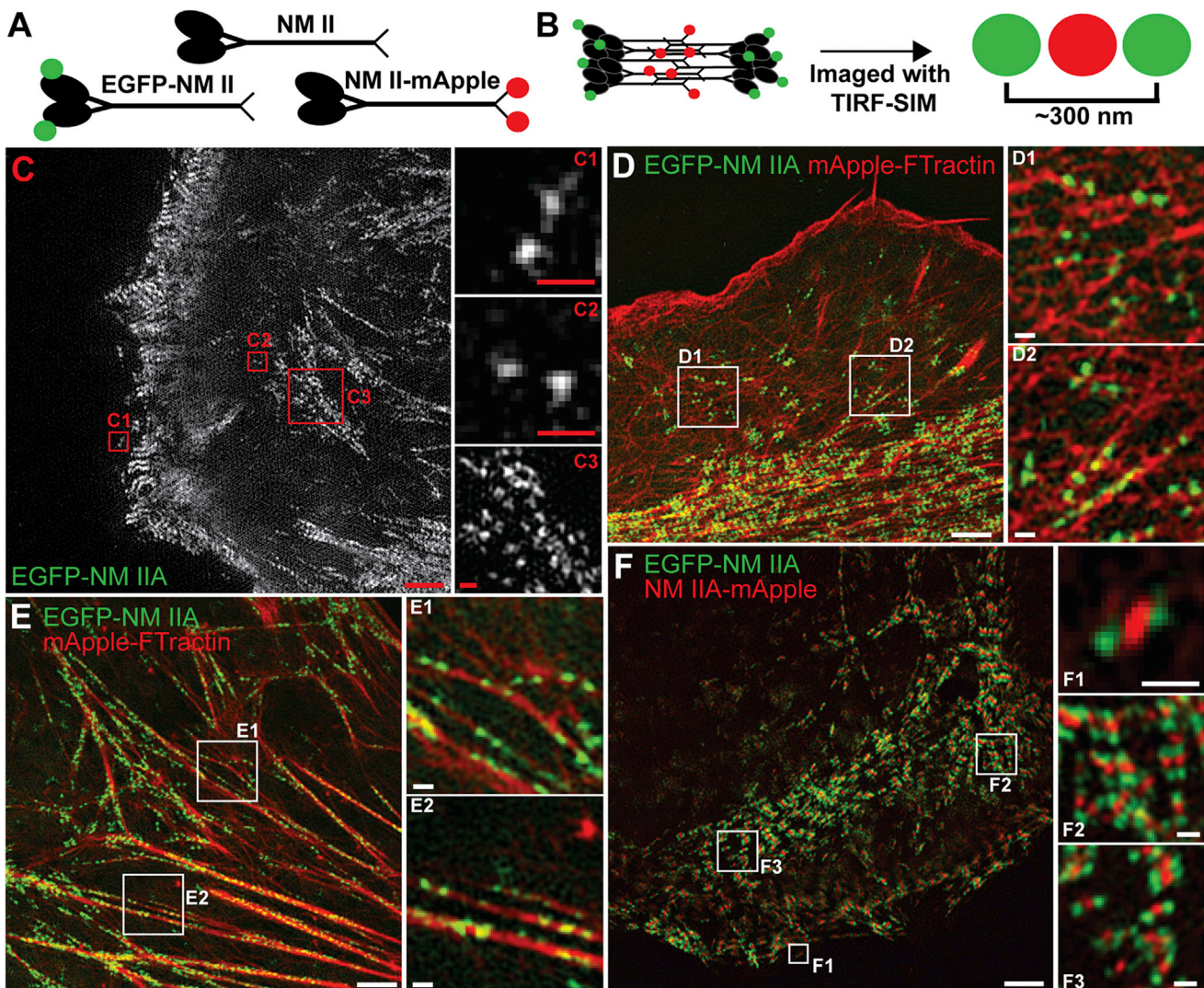


Figure 1. TIRF-SIM of Cells Expressing NM IIA with N- and C-Terminal Fluorescent Tags Allows Identification of Individual NM IIA Bipolar Filaments (A) Cartoon of NM II alone, with an N-terminal EGFP reporter, or with a C-terminal mApple reporter (light chains not depicted). (B) Cartoon of a NM II bipolar filament containing a combination of the three NM II constructs pictured in (A). To the right of the filament is a cartoon depicting what one would expect to see when such a filament is imaged with TIRF-SIM. (C) TIRF-SIM image of a U2OS cell expressing EGFP-NM IIA. Red numbered boxes correspond to the magnified insets to the right. Scale bars represent 2 μm for (C) and 300 nm for (C1)–(C3). (D and E) TIRF-SIM images of U2OS cells expressing EGFP-NM IIA and the F-actin reporter mApple-F-tractin. White numbered boxes correspond to the insets to the right. Scale bars represent 2 μm for (D) and (E) and 300 nm for insets. (F) TIRF-SIM image of a U2OS cell coexpressing EGFP-NM IIA and NM IIA-mApple. White numbered boxes correspond to the magnified insets to the right. Scale bars represent 2 μm for (F) and 300 nm for (F1)–(F3).

filaments were also very common in regions of the cell where NM II is highly enriched, such as in transverse arcs (Figure 2C and inset C2), ventral stress fibers (Figure 2D and insets D1 and D2), and subnuclear stress fibers (Figure 2E and insets E1 and E2). Heterotypic filaments were also present in peripheral lamella where NM IIB is much less abundant (Figure 2C and arrow in inset C1). Similar results were obtained using other cell types, including MDA-MB-231 and LLC-Pk1 cells (Figures S2A–S2C). Interestingly, time-lapse imaging revealed that the signal for NM IIB increases in many NM IIA-containing filaments as they move in retrograde fashion through the lamella (Movie S1). Finally, the fact that the position of the centroid of the red punctum relative to a line connecting the centroids of the two outer green puncta does not differ

significantly in cells coexpressing NM IIA-mApple and EGFP-NM IIB versus cells coexpressing NM IIA-mApple and EGFP-NM IIA (Figures S2D and S2E) argues that the green-red-green signals seen in Figure 2 correspond to heterotypic filaments and not homotypic filaments of NM IIA and NM IIB in close proximity to one another.

NM IIC is the most distantly related of the three NM II isoforms [23], raising the possibility that it does not coassemble with either NM IIA or NM IIB. To address this, we coexpressed NM IIC labeled with EGFP at its C terminus (NM IIC-EGFP) and NM IIA labeled with mApple at its N terminus (mApple-NM IIA). Similar to the results with NM IIA and NM IIB, NM IIA and NM IIC formed heterotypic filaments throughout U2OS cells, including at the leading edge (Figure S2F and inset F1), in

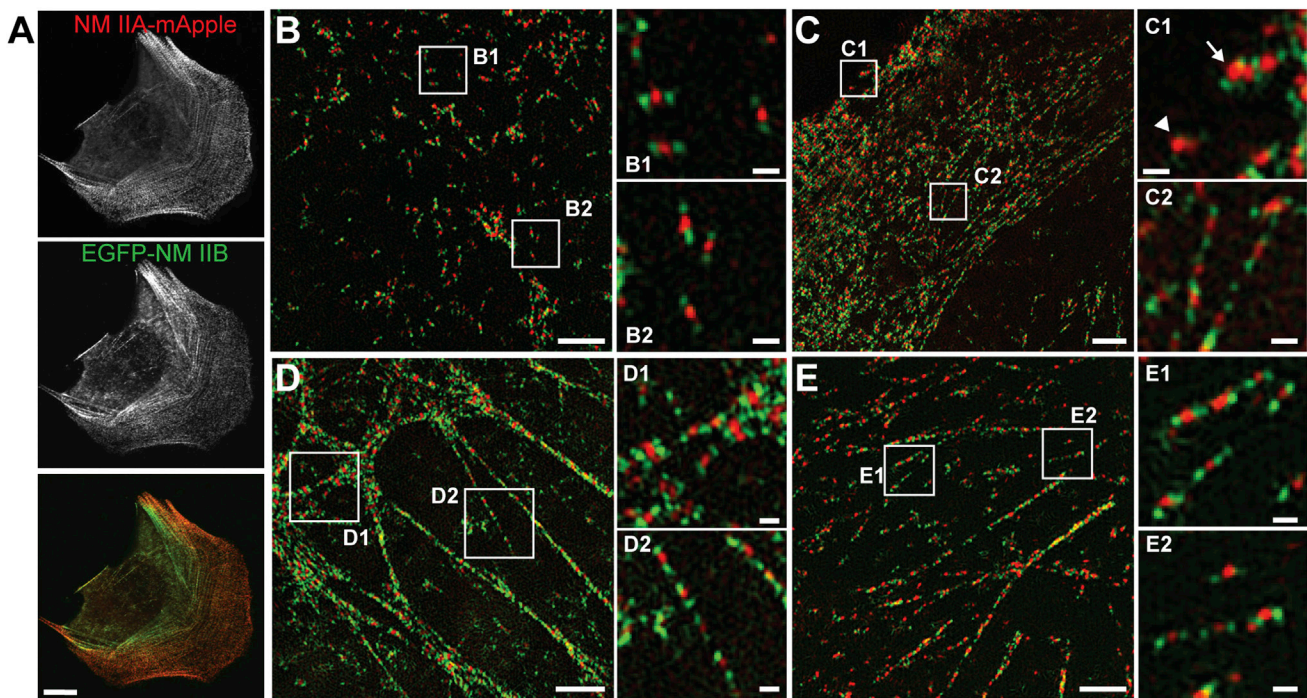


Figure 2. NM IIA and NM IIB Form Heterotypic Filaments in Live Cells

U2OS cells coexpressing NM IIA-mApple and EGFP-NM IIB were imaged using either confocal microscopy (A) or TIRF-SIM (B–E). For each TIRF-SIM image, the white numbered boxes correspond to the magnified insets to the right. Heterotypic filaments are apparent in regions of the cell without stress fibers (B), in lamellar extensions and transverse arcs (C), in ventral stress fibers (D), and in subnuclear stress fibers (E). In inset C1, the white arrowhead indicates a filament with little or no signal for EGFP-NM IIB (which could be either a homotypic filament of myosin IIA or a heterotypic filament containing unlabeled NM IIB or too few molecules of EGFP-NM IIB to be clearly visible; see [Experimental Procedures](#) for further discussion). Scale bar represents 10 μm in (A), 2 μm for the larger images in (B)–(E), and 300 nm for the insets in (B)–(E). See also [Figures S1](#) and [S2](#).

transverse arcs ([Figure S2F](#) and inset F2), and in ventral stress fibers ([Figure S2G](#) and insets G1 and G2). Collectively, these data show that all three NM II isoforms form heterotypic filaments in living cells. Also, because smooth muscle myosin II is more similar to NM IIA and NM IIB than NM IIC is to NM IIA and NM IIB [23], future efforts might address the possibility that smooth and nonmuscle myosins form heterotypic filaments to some extent, as suggested by previous *in vitro* experiments [9].

Heterotypic Filaments Are Present in the Contractile Ring

To determine whether heterotypic filaments also exist in the contractile ring of dividing cells, we used LLC-Pk1 cells. These cells have the advantage that they remain surface attached throughout most of cell division [24], allowing portions of the contractile ring to be visualized by TIRF-SIM. [Movie S2](#) shows that the contractile ring can be imaged effectively in TIRF-SIM through late anaphase in LLC-Pk1 cells expressing EGFP-NM IIA and mApple-F-tractin. Importantly, the green-red-green pattern indicative of heterotypic filaments is present within and around TIRF-accessible regions of the contractile ring (cleavage furrow marked by white arrows) in both early anaphase ([Figure 3A](#) and insets A1–A3) and mid-late anaphase ([Figure 3B](#) and insets B1–B3) in LLC-Pk1 cells expressing NM IIA-mApple and EGFP-NM IIB. Together, these results show that NM II isoforms also coassemble into heterotypic filaments in the contractile ring of dividing cells.

Endogenous NM II Isoforms Form Heterotypic Filaments

To determine whether endogenous NM II isoforms also form heterotypic filaments, we made use of NM II isoform-

specific antibodies that recognize the C-terminal nonhelical tailpieces of NM IIA or NM IIB. In the first experiment, we expressed EGFP-NM IIA in COS-7 cells (which normally express NM IIB and a small amount of NM IIC [6]) and then immunostained the cells for NM IIB. The cartoon in [Figure 4A](#) shows the green-red-green signal expected for heterotypic filaments of EGFP-NM IIA and endogenous NM IIB (detected using a red secondary antibody). [Figure 4C](#) and insets C1 and C2 show that endogenous NM IIB indeed formed heterotypic filaments with EGFP-NM IIA throughout TIRF-accessible regions of the cell. Similar results were obtained in MDA-MB-231 cells ([Figure S3A](#) and insets A1 and A2). Additionally, imaging of this MDA-MB-231 sample with 3D-SIM showed that isoform coassembly is not restricted to the TIRF zone, as heterotypic filaments were evident nearly 3 μm above the coverslip ([Figure S3B](#) and insets B1 and B2). Together, these results show that an endogenous NM II isoform can coassemble with a fluorescently tagged, exogenous NM II isoform and that antibodies recognizing the nonhelical tailpiece can be used to identify individual NM II filaments using SIM.

To demonstrate that endogenous NM IIA and endogenous NM IIB form heterotypic filaments, we double-stained polarized MDA-MB-231 cells, which express reasonable amounts of both isoforms [25], with a rabbit polyclonal antibody to the nonhelical tailpiece of NM IIA and a mouse monoclonal antibody to the nonhelical tailpiece of NM IIB. The cartoon in [Figure 4B](#) shows the single yellow puncta expected for heterotypic filaments composed of endogenous NM IIA and endogenous NM IIB (detected with green and red

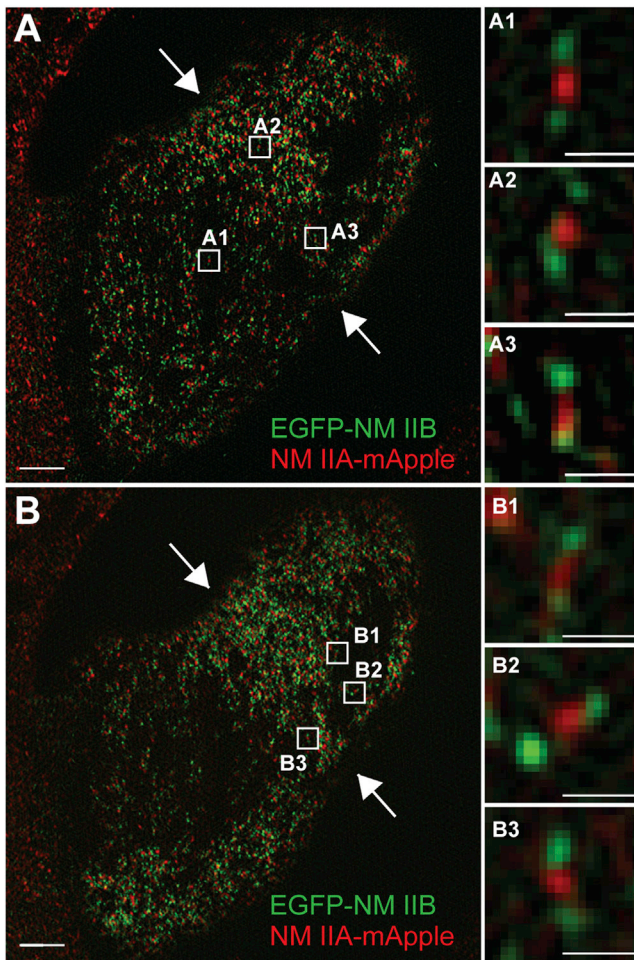


Figure 3. NM IIA and NM IIB Form Heterotypic Filaments in the Contractile Ring of LLC-Pk1 Cells

LLC-Pk1 cells expressing NM IIA-mApple and EGFP-NM IIB were imaged during anaphase using TIRF-SIM. The two images are of the same cell at early anaphase (A) and mid-late anaphase (B). White arrows indicate the position of the forming cleavage furrow. The numbered boxes in the larger images correspond to the magnified insets to the right. Scale bars represent 2 μm for larger images and 300 nm for insets. See also [Movie S2](#).

secondary antibodies, respectively), although yellow puncta with closely associated red and green signals could also correspond to heterotypic filaments for a variety of reasons (see the legend to [Figure 4](#) for details). Confocal micrographs of double-stained cells ([Figure S3C](#)) revealed that, as with overexpressed, tagged versions of NM IIA and NM IIB ([Figure 2A](#)), endogenous NM IIA and NM IIB “colocalize” to some degree throughout most of the cell. Most importantly, TIRF-SIM images of double-stained cells revealed signals that correspond to heterotypic filaments (i.e., yellow puncta with various amounts of closely associated red and green signals; see arrowheads) in areas rich in transverse arcs ([Figure 4D](#) and inset D1), in lamella ([Figure 4D](#) and inset D2), and in ventral stress fibers ([Figure 4E](#) and insets E1 and E2). Finally, MDA-MB-231 cells double stained with both the mouse monoclonal and a rabbit polyclonal antibody to the nonhelical tailpiece of NM IIB yielded signals ([Figure S3D](#) and insets D1 and D2) very similar to those observed when MDA-MB-231 cells were double stained for NM IIA and NM IIB. This observation supports our conclusion that the

yellow puncta possessing various amounts of closely associated red and green signals seen in [Figure 4](#) correspond to heterotypic filaments of endogenous NM IIA and NM IIB. Together, these results argue strongly that endogenous NM II isoforms coassemble into heterotypic filaments in living cells.

The Differential Distribution of NM IIA and NM IIB in Polarized Cells Is Reflected in the Composition of Individual Filaments

Numerous studies [[8](#), [20](#), [21](#)] have reported that NM IIA is enriched in peripheral lamella relative to NM IIB, whereas NM IIB is enriched in central and posterior regions relative to NM IIA. Our own confocal micrographs of well-polarized U2OS and MDA-MB-231 cells support this generalization ([Figures 2A](#) and [S3C](#)), although some NM IIB signal is clearly present in peripheral lamella where NM IIA is enriched, and some NM IIA is clearly present in interior regions where NM IIB is enriched. To determine whether this differential distribution of NM IIA and NM IIB is reflected in the composition of individual filaments, we quantitated TIRF-SIM images for the relative levels of endogenous NM IIA and NM IIB within individual filaments in well-polarized MDA-MB-231 cells stained with isoform-specific antibodies (see [Experimental Procedures](#) and the legends to [Figures 4](#) and [S4](#) for additional details). [Figure 4F](#) shows that the ratio of NM IIA to NM IIB in individual filaments is indeed dramatically in favor of NM IIA in peripheral lamella, and that this ratio diminishes progressively the further the filament is from the leading edge, eventually favoring NM IIB for interior filaments. Similar results were obtained when we scored the relative levels of exogenous NM IIA and NM IIB within individual filaments in well-polarized U2OS cells coexpressing NM IIA-mApple and EGFP-NM IIB ([Figure S4A](#), black bars). Together, these results argue strongly that the differential distribution of NM IIA and NM IIB seen in well-polarized cells is reflected in the composition of individual bipolar filaments. Moreover, the similarity in relative NM II isoform ratios reported in [Figures 4F](#) and [S4A](#) (black bars) argues that exogenously expressed isoforms largely reflect the properties of the endogenous proteins and can be used to further investigate the differential distribution of NM IIA and NM IIB.

The Differential Distribution of NM IIA and NM IIB May Be Driven by a Sorting Mechanism Acting over Time

In a final experiment, we sought to analyze the composition of individual filaments in freshly spread cells that are generating nascent lamella. Confocal micrographs of U2OS cells coexpressing NM IIA-mApple and EGFP-NM IIB and imaged 20 min after the initiation of spreading ([Figure S4B](#)) showed obvious increases in both the intensity of NM IIB and its degree of “colocalization” with NM IIA in peripheral lamella relative to mature peripheral lamella in cells that were fully polarized ([Figure 2A](#)). Moreover, TIRF-SIM revealed numerous heterotypic filaments within such nascent lamella ([Figure S3C](#) and insets C1–C3), suggesting that the increase in “colocalization” within nascent lamella corresponded to an increase in the amount of NM IIB relative to NM IIA within individual heterotypic filaments compared to mature lamella. This was borne out by scoring the TIRF-SIM images for the relative levels of exogenous NM IIA and NM IIB within individual filaments in nascent lamella ([Figure S4A](#); compare the red “spreading” bars to the black “polarized” bars). Indeed, the relative ratio of NM IIA to NM IIB in individual filaments in spreading cells remained much closer to 1 at nearly all distances from the cell edge as

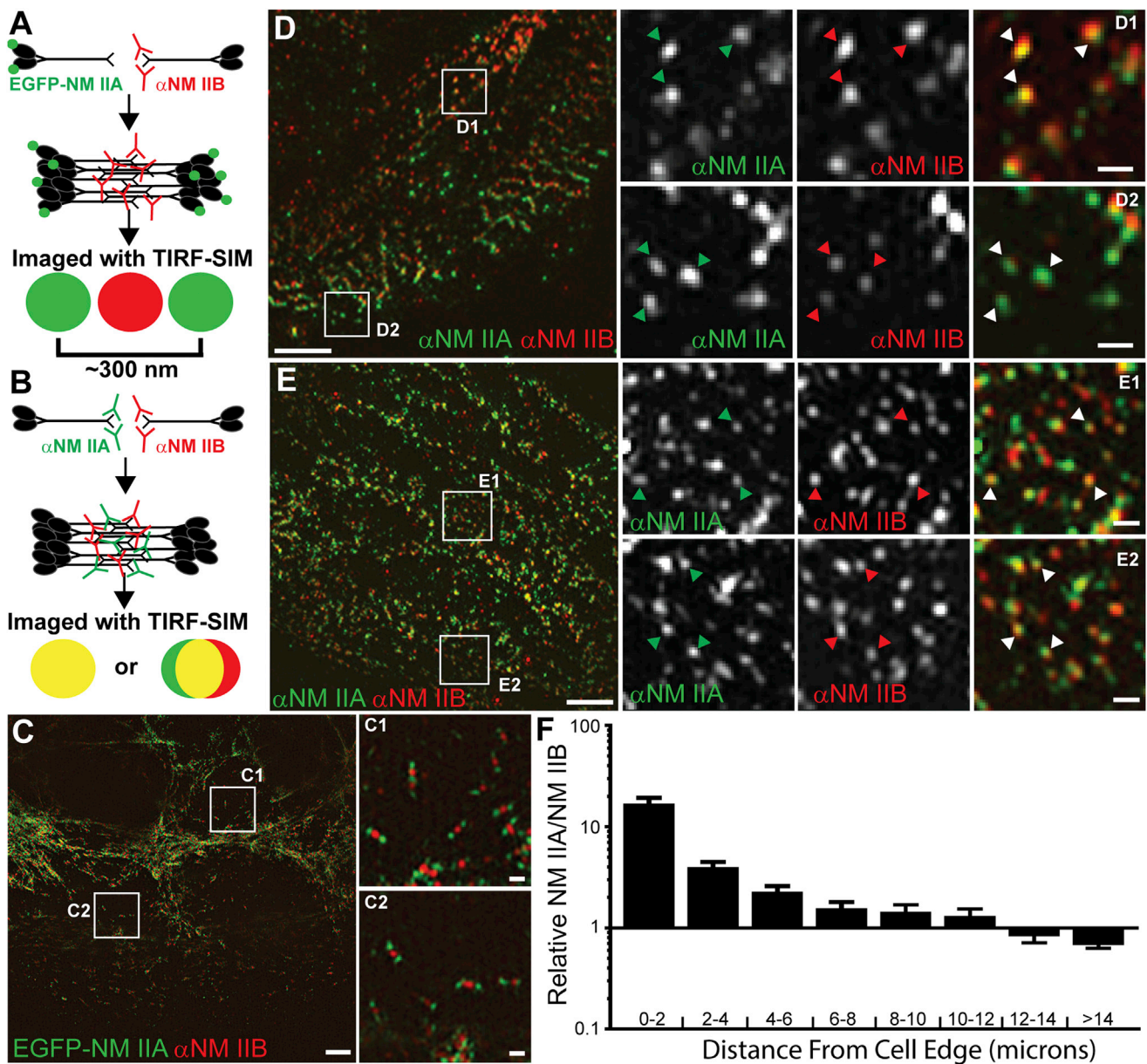


Figure 4. Endogenous NM IIA and NM IIB Form Heterotypic Filaments in Live Cells

(A) Cartoon depicting the coassembly of EGFP-NM IIA with endogenous NM IIB. When NM IIB is localized using an antibody that recognizes its C terminus (together with a red secondary antibody; red Y), the resulting heterotypic filament will display a green-red-green pattern when imaged with TIRF-SIM.

(B) Cartoon depicting the coassembly of endogenous NM IIA and endogenous NM IIB filament. Staining with antibodies that recognize the C termini of both NM IIA and NM IIB, together with green (green Y) and red (red Y) secondary antibodies, respectively, should result in a strong overlap between the two signals when heterotypic filaments are present. If both signals are of equal intensity and perfectly overlapping, the result will be a single yellow punctum. Any offset in the two signals will result in a punctum with a yellow center and red and green flanking regions. Signal offset could result from steric hindrance between adjacent antibodies, uneven labeling of filaments by the antibodies, and/or uneven distribution of isoforms on either side of the bipolar filament. In addition, the intensity of the yellow signal will be diminished in heterotypic filaments where the signal for one isoform is much stronger than the signal for the other isoform.

(C) COS-7 cells expressing EGFP-NM IIA were fixed, immunostained for endogenous NM IIB (followed by a red secondary), and imaged with TIRF-SIM. White numbered boxes correspond to the magnified insets to the right. Scale bars represent $2 \mu\text{m}$ for the larger image and 300 nm for the insets.

(D–F) MDA-MB-231 cells were fixed, immunostained with a rabbit polyclonal antibody for endogenous NM IIA (followed by a green secondary) and a mouse monoclonal antibody for endogenous NM IIB (followed by a red secondary), and imaged with TIRF-SIM.

(D and E) TIRF-SIM images of lamellar regions, transverse arcs, and ventral stress fibers. The numbered boxes correspond to the row of images to the right, which present grayscale images for α NM IIA and α NM IIB and the merged image. Arrowheads indicate some of the overlapping green and red puncta indicative of heterotypic filaments. Note that yellow is not obvious in D2 because the signal for NM IIA is much stronger than the signal for NM IIB. Scale bars represent $2 \mu\text{m}$ for the larger images and 300 nm for insets.

(F) Discrete individual puncta were analyzed for their relative content of endogenous NM IIA and NM IIB, and the results were plotted as a function of distance from the cell edge in $2 \mu\text{m}$ increments (see [Experimental Procedures](#) for details). The data, which are plotted on a log scale as geometric means with 95% confidence intervals, are a compilation of over 8,800 puncta from six cells. Note that the ratios in (F) are relative and do not necessarily represent the actual ratio of NM IIA to NM IIB in individual filaments due to differences in expression and assembly levels (see [Experimental Procedures](#)).

See also [Figures S3](#) and [S4](#).

compared to polarized cells. Therefore, freshly spread cells have a much more even distribution of NM IIA and NM IIB within individual filaments than polarized cells do.

The above data argue that, following initial spreading, a sorting mechanism operates over time to drive the differential composition of NM IIA and NM IIB within individual filaments observed in well-polarized cells. Previous studies have shed light on the sorting mechanism that might drive this differential distribution. First, swapping the C-terminal, assembly-competent domains of NM IIA and NM IIB largely reverses their differential distribution in polarized cells [8]. This important observation argues that the sorting process is assembly dependent. Second, fluorescence recovery after photobleaching (FRAP) analyses show that NM IIA present within filaments turns over more rapidly than NM IIB within filaments [8]. Moreover, a much higher percentage of total cellular NM IIA is in the soluble, monomeric form than is the case for NM IIB [8]. Finally, NM IIB's duty ratio (the fraction of a motor's catalytic cycle when it is bound to actin) is significantly higher than NM IIA's duty ratio [26, 27]. Based on these observations and the data reported here, we suggest the following scenario for how the differential distribution of NM IIA and NM IIB is established over time: (1) upon initial spreading, NM IIA and NM IIB are activated for assembly in lamellar extensions, where they coassemble; and (2) because of their differential stability within filaments, as filaments move rearward via retrograde flow, NM IIB will tend to remain within filaments, whereas monomers of NM IIA will tend to be released and recycled to peripheral regions for incorporation into new filaments. Layered over this sorting mechanism is, of course, the influence of differences in the total cellular contents of NM IIA and NM IIB. Factors such as Mts1 binding [28] and NM II heavy-chain phosphorylation [28, 29] could also contribute to the increased availability of NM IIA for filament assembly in peripheral regions. It also remains possible that differential assembly mediated by isoform-specific RLC phosphorylation contributes to some degree to the sorting mechanism [2].

Conclusions

The data presented here resolve a longstanding question in the myosin field regarding the molecular composition of NM II bipolar filaments *in vivo*. Considering the myriad cellular functions attributed to NM II, our unequivocal identification of heterotypic filaments within many actin-based structures inside living cells has broad implications. For example, efforts to parse out the contributions made by individual isoforms to overall NM II functions must now take into account heterotypic filament formation. Although the situation may be simplified in some contexts by the preferential or sole expression of a single NM II isoform, most cell types express multiple isoforms [3, 5]. This fact, together with our demonstration that when multiple NM II isoforms intermingle they form heterotypic filaments, argues that many functions attributed to NM II are being performed by heterotypic filaments. The properties of these mixed filaments are unknown and potentially complex. Future *in vitro* work exploring the biophysical properties of heterotypic filaments made using purified, full-length NM II isoforms will be required to resolve these issues.

Experimental Procedures

Microscopy

Confocal images were acquired using a Zeiss LSM 780 laser scanning confocal microscope equipped with a Zeiss 63×/1.4 NA oil objective.

TIRF-SIM imaging was performed using a Zeiss Axio Observer.Z1 inverted microscope outfitted with an apparatus enabling structured illumination [30]. The key component in this structured-illumination apparatus is a spatial light modulator (SLM) that functions as a phase grating with submillisecond pattern switching speed [14, 30]. Two-color TIRF-SIM imaging requires that the excitation beams of the two different wavelengths be confined within the TIRF annulus at the objective's back focal plane. The SLM is capable of this because it can change the diffraction angles for different excitation wavelengths by loading patterns of different periods. An Olympus 100×/1.49 NA (Olympus) objective was used instead of the Zeiss 1.45 NA objective because the slightly larger NA of the Olympus objective gives higher tolerance for placing the excitation beams inside the TIRF annulus. The high-NA TIRF objective also provides an increase in resolution over standard 3D-SIM. Reconstructed TIRF-SIM images were generated from the raw data as described previously [14]. For two-color TIRF-SIM, each channel was captured on a separate sCMOS camera, and image registration was performed on reconstructed images using the alignment function in Prism (UCSF). 3D-SIM imaging was performed on a DeltaVision OMX 3D-SIM Imaging System (Applied Precision) equipped with an Olympus 60×/1.42 NA objective. Raw images were reconstructed using Softworx software (Applied Precision). Linear adjustments were made to images using ImageJ.

Quantitation of Relative NM IIA/NM IIB in Individual Filaments

For Figure 4F, TIRF-SIM images of well-polarized MDA-MB-231 cells that had been immunostained for both NM IIA and NM IIB were used for analysis. For Figure S4A, TIRF-SIM images of U2OS cells expressing EGFP-NM IIB and NM IIA-mApple that had been allowed to polarize ("polarized") or were trypsin treated, replated on coverslips, and imaged between 20 and 40 min postplating ("spreading") were used for analysis. Integrated pixel intensities in both the red and green channels were measured inside a 230 nm circle drawn in ImageJ around discrete red and/or green puncta for Figure 4F, and inside a 450 nm circle around discrete NM IIA-mApple puncta for Figure S4A. The integrated pixel intensities for individual filaments were then divided by the integrated pixel intensity in each channel for the entire image to provide the percentage of the total intensity in each channel that is present within each individual filament. The percentage of the total for NM IIA was then divided by the percentage of the total for NM IIB to give the relative NM IIA to NM IIB ratio in each individual filament. The distance of each punctum from the leading edge was also determined. For "Spreading" cells, the leading edge was considered the nearest cell edge. The ratios were then grouped into 2 μm bins based on distance from the leading edge. Because the final numbers are ratios, calculating mean values would skew the data in favor of the numerator. Therefore, we plotted the data on a log scale as geometric means with 95% confidence intervals. Image analysis was performed with ImageJ, and the data were plotted using GraphPad Prism. We note that although some of the filaments in this quantitative analysis are probably homotypic, the unequivocal scoring of filaments as homotypic is problematic because of the presence of endogenous proteins, the potential for misfolded fluorophores, and the technical limitations in trying to identify one or a few fluorophores. It is also important to note that the ratios reported in Figures 4F and S4A are relative values and do not necessarily represent that actual ratio of NM IIA to NM IIB in individual filaments due to differences in expression and assembly levels.

Supplemental Information

Supplemental Information includes four figures, one table, Supplemental Experimental Procedures, and two movies and can be found with this article online at <http://dx.doi.org/10.1016/j.cub.2014.03.071>.

Acknowledgments

The authors would like to thank Tom Egelhoff, Xuefei Ma, and Bob Adelstein for reagents; Xufeng Wu (NHLBI Light Microscopy Core) for imaging advice and facilitating our collaborations; Helen White for assistance with the LLC-Pk1 experiments; Jim Sellers for discussions; and the NHLBI Flow Cytometry Core.

Received: January 3, 2014

Revised: March 25, 2014

Accepted: March 27, 2014

Published: May 8, 2014

References

1. Vicente-Manzanares, M., Ma, X., Adelstein, R.S., and Horwitz, A.R. (2009). Non-muscle myosin II takes centre stage in cell adhesion and migration. *Nat. Rev. Mol. Cell Biol.* **10**, 778–790.
2. Sandquist, J.C., Swenson, K.I., Demali, K.A., Burrige, K., and Means, A.R. (2006). Rho kinase differentially regulates phosphorylation of nonmuscle myosin II isoforms A and B during cell rounding and migration. *J. Biol. Chem.* **281**, 35873–35883.
3. Tullio, A.N., Accili, D., Ferrans, V.J., Yu, Z.X., Takeda, K., Grinberg, A., Westphal, H., Preston, Y.A., and Adelstein, R.S. (1997). Nonmuscle myosin II-B is required for normal development of the mouse heart. *Proc. Natl. Acad. Sci. USA* **94**, 12407–12412.
4. Kim, K.Y., Kovács, M., Kawamoto, S., Sellers, J.R., and Adelstein, R.S. (2005). Disease-associated mutations and alternative splicing alter the enzymatic and motile activity of nonmuscle myosins II-B and II-C. *J. Biol. Chem.* **280**, 22769–22775.
5. Bao, J., Ma, X., Liu, C., and Adelstein, R.S. (2007). Replacement of nonmuscle myosin II-B with II-A rescues brain but not cardiac defects in mice. *J. Biol. Chem.* **282**, 22102–22111.
6. Bao, J., Jana, S.S., and Adelstein, R.S. (2005). Vertebrate nonmuscle myosin II isoforms rescue small interfering RNA-induced defects in COS-7 cell cytokinesis. *J. Biol. Chem.* **280**, 19594–19599.
7. Conti, M.A., Even-Ram, S., Liu, C., Yamada, K.M., and Adelstein, R.S. (2004). Defects in cell adhesion and the visceral endoderm following ablation of nonmuscle myosin heavy chain II-A in mice. *J. Biol. Chem.* **279**, 41263–41266.
8. Sandquist, J.C., and Means, A.R. (2008). The C-terminal tail region of nonmuscle myosin II directs isoform-specific distribution in migrating cells. *Mol. Biol. Cell* **19**, 5156–5167.
9. Pollard, T.D. (1975). Electron microscopy of synthetic myosin filaments. Evidence for cross-bridge. Flexibility and copolymer formation. *J. Cell Biol.* **67**, 93–104.
10. Sato, M.K., Takahashi, M., and Yazawa, M. (2007). Two regions of the tail are necessary for the isoform-specific functions of nonmuscle myosin IIB. *Mol. Biol. Cell* **18**, 1009–1017.
11. Rosenberg, M., Straussman, R., Ben-Ya'acov, A., Ronen, D., and Ravid, S. (2008). MHC-IIB filament assembly and cellular localization are governed by the rod net charge. *PLoS ONE* **3**, e1496.
12. Beach, J.R., and Egelhoff, T.T. (2009). Myosin II recruitment during cytokinesis independent of centralspindlin-mediated phosphorylation. *J. Biol. Chem.* **284**, 27377–27383.
13. Ricketson, D., Johnston, C.A., and Prehoda, K.E. (2010). Multiple tail domain interactions stabilize nonmuscle myosin II bipolar filaments. *Proc. Natl. Acad. Sci. USA* **107**, 20964–20969.
14. Kner, P., Chhun, B.B., Griffis, E.R., Winoto, L., and Gustafsson, M.G. (2009). Super-resolution video microscopy of live cells by structured illumination. *Nat. Methods* **6**, 339–342.
15. Niederman, R., and Pollard, T.D. (1975). Human platelet myosin. II. In vitro assembly and structure of myosin filaments. *J. Cell Biol.* **67**, 72–92.
16. Billington, N., Wang, A., Mao, J., Adelstein, R.S., and Sellers, J.R. (2013). Characterization of three full-length human nonmuscle myosin II paralogs. *J. Biol. Chem.* **288**, 33398–33410.
17. Ebrahim, S., Fujita, T., Millis, B.A., Kozin, E., Ma, X., Kawamoto, S., Baird, M.A., Davidson, M., Yonemura, S., Hisa, Y., et al. (2013). NMII forms a contractile transcellular sarcomeric network to regulate apical cell junctions and tissue geometry. *Curr. Biol.* **23**, 731–736.
18. Johnson, H.W., and Schell, M.J. (2009). Neuronal IP3 3-kinase is an F-actin-bundling protein: role in dendritic targeting and regulation of spine morphology. *Mol. Biol. Cell* **20**, 5166–5180.
19. Yi, J., Wu, X.S., Crites, T., and Hammer, J.A., 3rd. (2012). Actin retrograde flow and actomyosin II arc contraction drive receptor cluster dynamics at the immunological synapse in Jurkat T cells. *Mol. Biol. Cell* **23**, 834–852.
20. Kolega, J. (1998). Cytoplasmic dynamics of myosin IIA and IIB: spatial 'sorting' of isoforms in locomoting cells. *J. Cell Sci.* **111**, 2085–2095.
21. Beach, J.R., Hussey, G.S., Miller, T.E., Chaudhury, A., Patel, P., Monslow, J., Zheng, Q., Keri, R.A., Reizes, O., Bresnick, A.R., et al. (2011). Myosin II isoform switching mediates invasiveness after TGF- β -induced epithelial-mesenchymal transition. *Proc. Natl. Acad. Sci. USA* **108**, 17991–17996.
22. Shutova, M., Yang, C., Vasiliev, J.M., and Svitkina, T. (2012). Functions of nonmuscle myosin II in assembly of the cellular contractile system. *PLoS ONE* **7**, e40814.
23. Golomb, E., Ma, X., Jana, S.S., Preston, Y.A., Kawamoto, S., Shoham, N.G., Goldin, E., Conti, M.A., Sellers, J.R., and Adelstein, R.S. (2004). Identification and characterization of nonmuscle myosin II-C, a new member of the myosin II family. *J. Biol. Chem.* **279**, 2800–2808.
24. Rusan, N.M., and Wadsworth, P. (2005). Centrosome fragments and microtubules are transported asymmetrically away from division plane in anaphase. *J. Cell Biol.* **168**, 21–28.
25. Betapudi, V., Gokulrangan, G., Chance, M.R., and Egelhoff, T.T. (2011). A proteomic study of myosin II motor proteins during tumor cell migration. *J. Mol. Biol.* **407**, 673–686.
26. Wang, F., Kovacs, M., Hu, A., Limouze, J., Harvey, E.V., and Sellers, J.R. (2003). Kinetic mechanism of non-muscle myosin IIB: functional adaptations for tension generation and maintenance. *J. Biol. Chem.* **278**, 27439–27448.
27. Kovács, M., Wang, F., Hu, A., Zhang, Y., and Sellers, J.R. (2003). Functional divergence of human cytoplasmic myosin II: kinetic characterization of the non-muscle IIA isoform. *J. Biol. Chem.* **278**, 38132–38140.
28. Dulyaninova, N.G., Malashkevich, V.N., Almo, S.C., and Bresnick, A.R. (2005). Regulation of myosin-IIA assembly and Mts1 binding by heavy chain phosphorylation. *Biochemistry* **44**, 6867–6876.
29. Breckenridge, M.T., Dulyaninova, N.G., and Egelhoff, T.T. (2009). Multiple regulatory steps control mammalian nonmuscle myosin II assembly in live cells. *Mol. Biol. Cell* **20**, 338–347.
30. Fiolka, R., Shao, L., Rego, E.H., Davidson, M.W., and Gustafsson, M.G. (2012). Time-lapse two-color 3D imaging of live cells with doubled resolution using structured illumination. *Proc. Natl. Acad. Sci. USA* **109**, 5311–5315.